2 Orogen-scale erosion

Definitions. The term denudation, which is derived from the latin denudare, means to make bare (Ring et al., 1999). In a geological context it refers to the exposure of rocks by erosion, but also involves the processes of weathering and transportation (Allaby and Allaby, 1999; Ring et al., 1999). Erosion, which is derived from the latin erodere, means to gnaw at or to crush something. In a geological context it refers to the physical and chemical breakdown of rocks and also involves the transport of the resulting materials (Allaby and Allaby, 1999). From the above definitions it is evident that they overlap, which leads to a widely synonymous use of both terms (Ring et al., 1999). There is however a tendency to restrict erosion to the local removal of rocks by rivers, glaciers or bedrock landslides. Accordingly, denudation would refer to the large scale exposure of bedrock (Leeder, 1991; Summerfield and Brown, 1998; Ahnert, 1999). On the contrary denudation is often used in the context of tectonic unroofing (Ring et al. (1999) and Sean Willett pers. com., (2004)). Given that there is no clear agreement upon the application of both terms, I follow Sean Willett and use the term erosion, since it is less ambiguous in its reference to physical or chemical surface processes.

Within this respect, the sediment supply system is commonly considered to be a product of the interaction between erosivity and erodibility. The former describes the potential of a river or glacier to remove material from a certain locality, i. e., the amount of abrasive tools transported within either the river, the glacier or even within the air. In contrast, erodibility refers to the resistance of a certain lithology to the work of the erosion agents. Erodibility depends on the physical and chemical composition of the lithology subject to erosion, the mechanic properties of the lithology, the infiltration capacity and climatic parameters such as temperature, temperature range, and availability of water (Hovius, 1998).

The term uplift refers to the displacement in the direction opposite to the gravity vector. A displacement is only defined when both, the object displaced and the frame of reference are specified. Accordingly, surface uplift is the displacement of Earth's surface with respect to the geoid (Fig. 2.1). Similarly, rock uplift is defined as the displacement of rocks with respect to the geoid. Displacement of rocks with respect to the surface is referred to as exhumation, where the exhumation rate equals the erosion rate or the rate of removal of overburden by tectonic processes. The above relation can also be written as:

$$\text{surface uplift} = \text{rock uplift} - \text{exhumation}. \quad (2.1)$$

It is emphasised here that the often implicitly made assumption that rock uplift equals surface uplift is equivalent to the assumption that the exhumation is zero – often a difficult assumption to justify (England and Molnar, 1990).

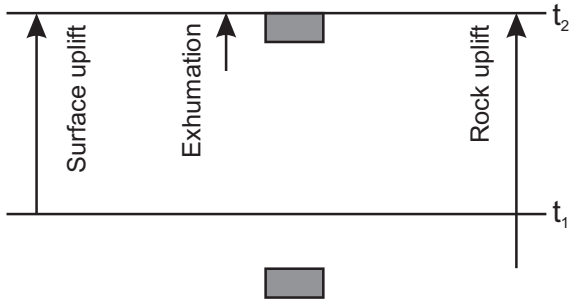

Figure 2.1: Graphic definition of key parameters describing vertical movements within Earth's crust. Taken from Burbank and Anderson (2001).

Erosion patterns. One implication of the subduction-accretion process is the tectonic advection of material towards the surface of a collisional orogen. The way of how the resulting topography is counteracted by rivers, glaciers, and bedrock landslides depends on a number of factors. Among

the most important ones are latitude and altitude of an orogen, its position with respect to global atmospheric and oceanic circulation systems, the erosivity of antecedent rivers, channel slope, orientation of topographic slope with respect to geologic structures, water discharge, erodibility, and rate of uplift (Selby, 1982; Seidl and Dietrich, 1992; Howard et al., 1994; Sugai et al., 1994; Hay, 1996; Schmidt and Montgomery, 1995; Hovius, 1998; Meigs and Sauber, 2000; Zeitler et al., 2001).

Given sufficient precipitation, a drainage network will cover the entire orogen up to the channel heads or the snow line. Thereby, the spacing of the transverse streams, which transport most of the material eroded within an orogen, is very regular and is linearly correlated with the half-width of the orogen (Hovius, 1996). This spacing does not differ significantly between young and old orogens and is thus independent of the age or the degree of maturity of an orogen, i. e., the collision stage. Nearly all orogens show at least in parts such a drainage network among them: the Southern Alps of New Zealand, Central Range in Taiwan, the Apennines in Italy, the Peruvian Andes, and the European Alps (Hovius, 1996). This regular organisation of drainage networks and the associated erosion is envisaged to be characteristic for a distributed erosion pattern (Fig. 2.2).

In contrast, monsoon derived precipitation may focus erosion as demonstrated by Wobus et al. (2003), Hodges et al. (2004), and Thiede et al. (2004). According to Thiede et al. (2004), more than 80 % of the annual precipitation ($> 2000\,mm/a$) of the Indian summer monsoon is forced out along the High Himalayan mountain front in NW India at elevations between ~ 2 and $3.5\,km$. This altitudinal band corresponds with an approximately $50-70\,km$ wide zone of high exhumation rates (Fig. 2.3). Furthermore, Thiede et al. (2004) and Bookhagen et al. (2005) showed that where monsoonal circulation reaches major N – S oriented valleys in the High Himalayas, moisture is channeled farther into the orogen and may lead to higher erosion rates along these valleys. A similar observation is derived from field

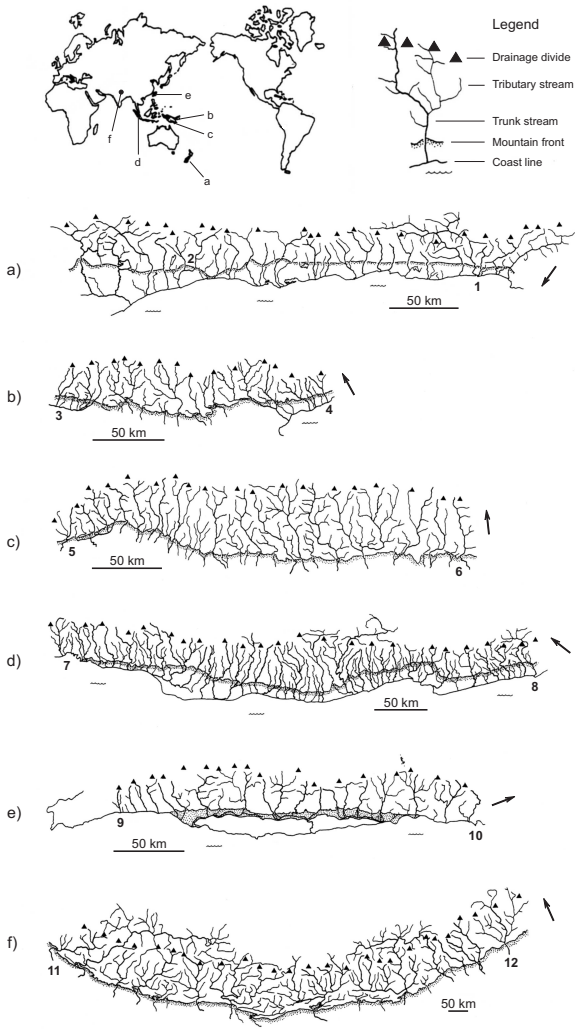

Figure 2.2: Drainage patterns in mountain belts, taken from Hovius (1996). Ranges: (a) Southern Alps, New Zealand; (b) Finisterre Range, Papua New Guinea; (c) Maoke range, Irian Jaya; (d) Barisan Range, Sumatra; (e) Central Range, Taiwan; (f) Himalaya, India/Nepal. Trunk streams: 1 Turnbull; 2 Styx; 3 Surinam; 4 Buham; 5 Ukemupuko; 6 Lorentz; 7 Bajang; 8 Manna; 9 Ta wu; 10 nameless; 11 Beas; 12 Manas. Arrow points to North.

studies in the Toro basin, which belongs to a series of intra-montane basins within the Eastern Cordillera. Hilley and Strecker (2005) pointed

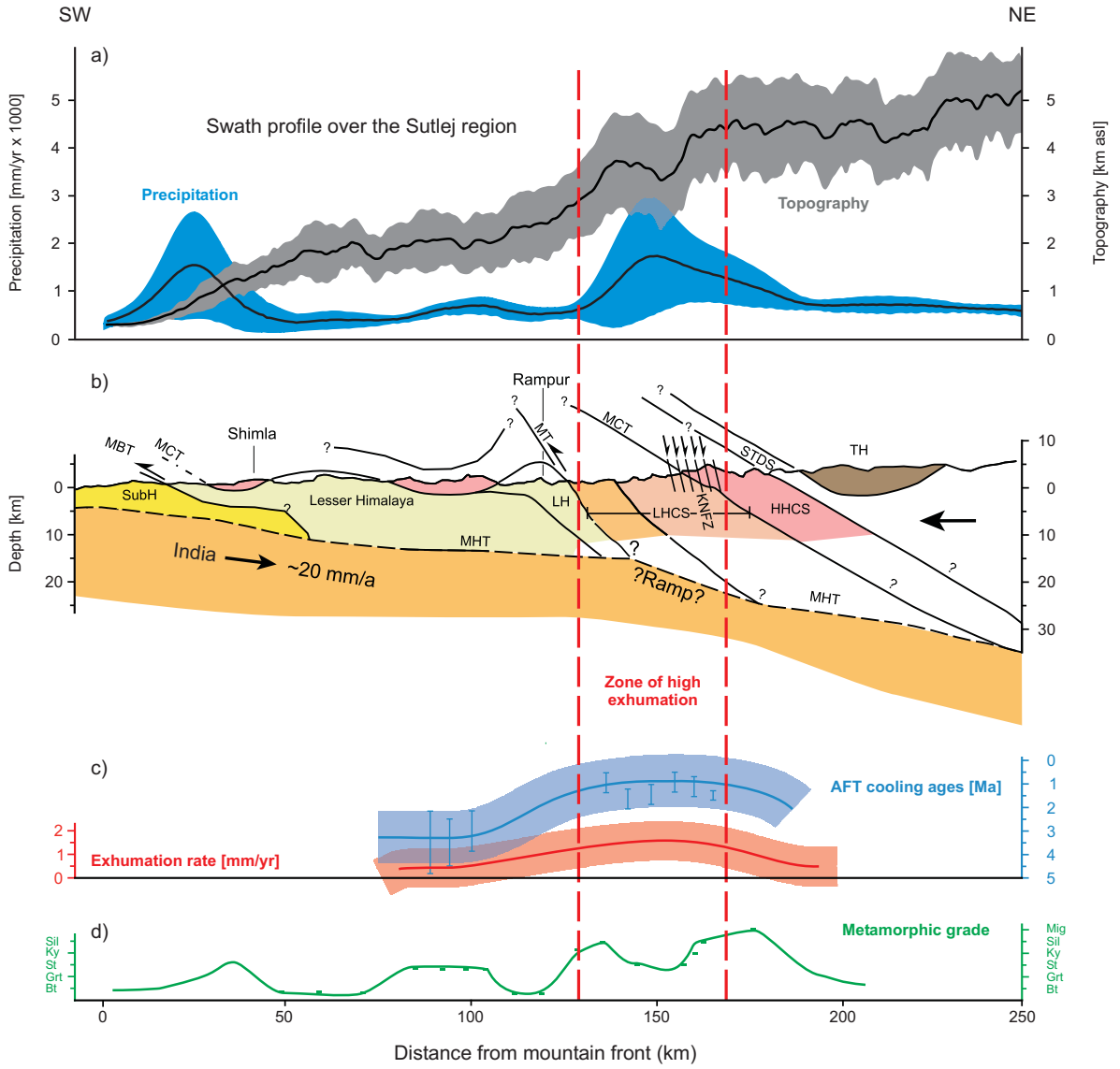

Figure 2.3: Example of focused erosion in the Himalayas. Modified after Thiede et al. (2004). (a) Compiled data illustrate the coupling between surface processes and deformation in the Sutlej Region. Topographic (grey) and precipitation - distribution (blue) swath profiles for the Sutlej area are oriented perpendicular to the SHF. Swath profiles: $250\,km$ long, $100\,km$ wide, thick, lines indicate mean values, shaded areas denote $\pm 2\sigma$. Distribution of orographic precipitation is focused between elevations of $\sim 2-3.5\,km$ in a $\sim 50-70\,km$-wide zone. (b) Simplified geologic cross-section parallels swath profile. (c) AFT cooling ages (blue) parallel to the geologic cross-section and estimated exhumation rates (red); lines indicate mean values, shaded areas denote $\pm 2\,\sigma$. (d) Metamorphic grade of the rocks along the profile line. Based on AFT cooling ages (c), the coincidence between rapid erosion and exhumation is focused in a $\sim 50-70\,km$-wide sector of the Himalayan orogenic belt. Enhanced and focused orographic precipitation (a) localized erosion and exhumation over geologic time and resulted in exhumation of high-grade metamorphic rocks (d) by motion along a back-stepping thrust to the south (MT) and normal fault zone (KNFZ) to the north (b). TH, Tethyan Himalaya; HHCS, High Himalayan Crystalline Sequence; LHCS, Lesser Himalayan Crystalline Sequence; LH, Lesser Himalaya; SUBH, Sub Himalaya; STFS, Southern Tibetan Fault System; MCT, Main Central Thrust; KNFZ, Karcham Normal Fault Zone; MT, Munsiari Thrust; MBT, Main Boundary Thrust; MHT, Main Himalayan Thrust.

out that the meridional orientation of the Eastern Cordillera concentrates moisture along its eastern flank, which leads to a steep precipitation gradient between the humid foreland ($\sim 1200\,mm/a$ mean annual precipitation) and the arid intra-montane Toro basin ($\sim 260\,mm/a$ mean annual precipitation). However, the outlet of the Rio Toro in the foreland allows penetration of moisture into the respective gorge and ultimately into the Toro basin itself (Hilley and Strecker, 2005).

In a likewise manner, the Southern Alps of New Zealand form an orographic barrier to the moisture laden, north-westerly winds moving off the Tasman Sea. Mean annual precipitation rates reach as much as $15\,m$ on the steep western flank of the orogen and resulted in erosion rates by landslides of up to $9\,mm/a$ and of likewise high rock uplift rates approaching $7\,mm/a$ (Hovius et al., 1997).

Antecedent rivers with high erosivity, which cross an orogen, might also focus erosion. Both the Indus and the Tsangpo river were capable of cutting steep gorges with several thousand meters relief into the massifs of Nanga Parbat and Namche Barwa, respectively (Zeitler et al., 2001; Koons et al., 2002). This focused erosion lead to the rapid exhumation of Quaternary metamorphic rocks and granites (Zeitler et al., 2001) and may also have attracted channel flow within the middle to lower crust (Zeitler et al., 2001; Beaumont et al., 2001). A further example of an antecedent river focussing deformation is provided by the Surkhob river (Pavlis et al., 1997). Since Late Miocene to Pliocene times the Surkhob river takes its course right above the northern deformation front of the Pamir and removed nearly all material delivered to this deformation front. According to Pavlis et al. (1997) this has lead to a halt in deformation front advance, to a build up of excess topography along the deformation front and to backthrusting as well as out-of-sequence thrusting.

Orogen-scale glacial erosion can also be considered as focused. Glacial erosion is at its maximum along the mean position of the Equilibrium Line Altitude (ELA), where the net mass balance of glaciers is equal to zero (i. e., accumulation equals ablation), the sliding velocity of glaciers is highest and so is the erosion rate. Below the ELA, glacial erosion decreases and fluvial processes start to dominate (Fig. 2.4). Due to the transition from warm-based to cold-based glaciers, the latter are frozen to their beds, at higher altitudes, glacial erosion decreases above the ELA (Meigs and Sauber, 2000; Burbank, 2002). One prominent example for this scenario is the Chugach/St. Elias Range in Southern Alaska, where high deformation and exhumation rates are confined to an altitudinal band spanned by the ELA (Meigs and Sauber, 2000; Sheaf et al., 2003; Spotila et al., 2004).

Based on the above observations we propose that orogen-scale erosion can either be envisaged as distributed or focused. These modes are considered as two alternatives of the spatial distribution of erosion. Given the sensitivity of crustal wedges to erosion as outlined in the preceding chapter, both erosion modes should evoke a characteristic deformation pattern.

Simulation of orogen-scale erosion. Several methods have been suggested to incorporate erosion into either numerical or physical simulations (e. g., Koons, 1995; Mugnier et al., 1997; Willett, 1999; Persson et al., 2004). In essence four classes of orogen-scale erosion models can be distinguished:

i. Erosion rate is constant through time and space (Fig. 2.5a)

$$v_{er} = -\frac{dH}{dt} = constant \qquad (2.2)$$

where v_{er} is the erosion rate, H is the elevation and t is time.

ii. Erosion rate is proportional to elevation (Fig. 2.5b)

$$v_{er} = -\frac{dH}{dt} = -\frac{H}{t_E} \qquad (2.3)$$

where the erosion parameter t_E (in units of time) describes how long it takes to erode a mountain of the elevation H.

iii. Erosion rate is proportional to slope (Fig. 2.5c)

$$v_{er} = -\frac{dH}{dt} = -\frac{u\,dH}{dx} \tag{2.4}$$

where x is a horizontal spatial coordinate and dH/dx is the topographic gradient, i. e., the slope. The proportionality constant u is the horizontal rate of displacement of the slope.

iv. Erosion rate is proportional to surface curvature (Fig. 2.5d)

$$q = -\frac{D\,dH}{dx} \tag{2.5}$$

where q is the rate of down slope transport of mass (mass flux), dH/dx is the topographic gradient, the slope and D is the erosional diffusivity.

The constant erosion approach (Eq. 2.2) is the most dramatic simplification of real erosion processes, but has been very successfully used to explain the clockwise shape of metamorphic PT paths (Stüwe, 2000). In sandbox simulations this model was applied by Mugnier et al. (1997), Leturmy et al. (2000), and Persson and Sokoutis (2002), who did not distinguish between pro- and retro-wedge erosion.

The elevation dependent erosion model (Eq. 2.3) is a variant of an assumption made by Ahnert (1970), which states that erosion rates increase with increasing local relief and that the latter is in turn positively correlated with elevation (Milliman and Syvitski (1992), Summerfield and Hulton (1994), Fig. 2.6). From a causal perspective this relation is generally invalid, since it is incompatible with fluvial incision laws. Also elevation by itself cannot be a determining factor (Peter Koons pers. com., (2004)). Additionally,

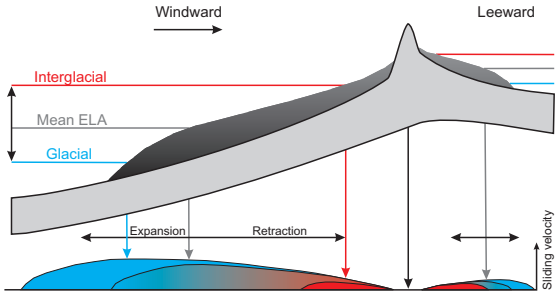

Figure 2.4: Model illustrating relationship between sliding velocity and the ELA across an orogenic belt. An orographically induced rise in ELA leads to a higher mean ELA (solid back) line. Smaller amplitude fluctuations of the ELA between glacial (blue) and interglacial (red) are shown schematically. Assuming that bedrock erosion rate scales with basal sliding velocity (Hallet et al., 1996), the model suggests concentration of erosion in a topographic band whose height is dictated by glacial/interglacial altitudinal limits to the ELA and whose width is a function of the concomitant glacial expansion/retraction in the landscape. The windward band width and height are likely to be greater than those of the leeward flank. The range crest is defined by a topographic peak that corresponds spatially with a zone of low glacial erosion. Modified after Meigs and Sauber (2000).

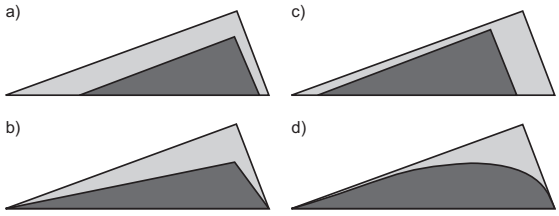

Figure 2.5: Influence of different erosion models on the shape of an asymmetric mountain belt. The light shaded area shows the mountain belt before, the dark shaded area after erosion. (a) Constant erosion rate. (b) Erosion rate proportional to elevation. (c) Erosion rate proportional to slope. (d) Erosion rate proportional to surface curvature. Note that the highest point of the topography remains laterally fixed in erosion models (a) and (b). Modified after Stüwe (2000).

an elevation dependent erosion model does not take other parameters like uplift or precipitation rates into account and thus contradicts with observations from recent field studies. Dadson et al. (2003) showed that the highest erosion rates in Taiwan are found where rapid deformation, high storm frequency and weak substrates coincide, despite low topographic relief. Nevertheless, an

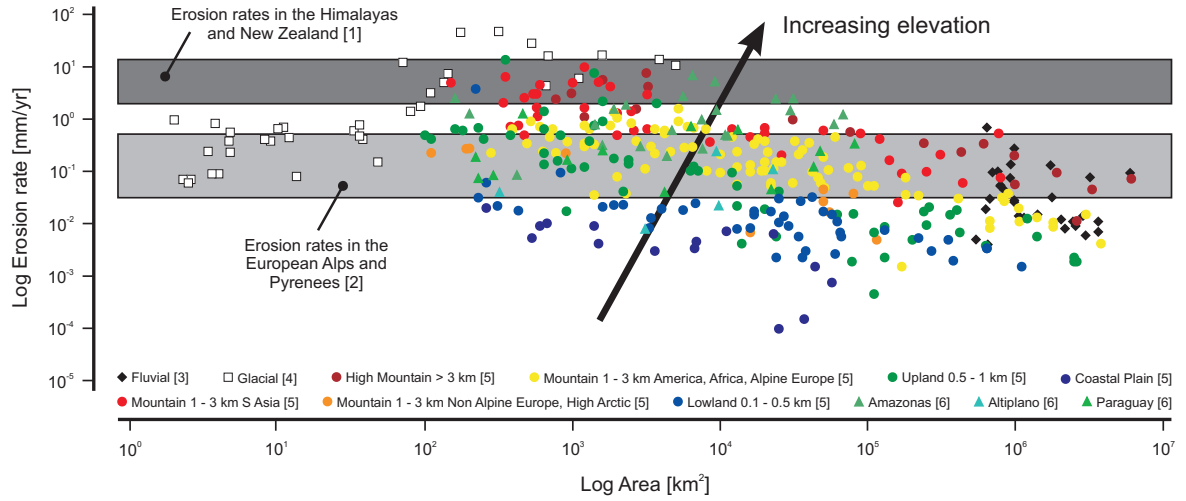

Figure 2.6: Relation between catchment area, erosion rate, and altitude (arrow). Note different trends for fluvial and glacial erosion rates. The latter are highest along the ELA and a larger catchment area implies a larger area covered by the ELA. A larger catchment area in fluvial terrains is often associated with low local relief, which hampers fluvial erosion. Data sources: [1] Adams (1980), Hovius et al. (1997), Lavé and Avouac (2001), Zeitler et al. (2001), White et al. (2002), Dadson et al. (2003), Willett et al. (2003), Barnard et al. (2004); [2] Morris et al. (1998), Fitzgerald et al. (1999), Schlunegger et al. (2001); [3] Summerfield and Hulton (1994); [4] Hallet et al. (1996); [5] Milliman and Syvitski (1992); [6] Filizola et al. (2002).

elevation dependent erosion model is a closer approximation of nature when compared with the constant erosion model (Stüwe, 2000).

The model, which states that erosion rates are proportional to slope (Eq. 2.4) was used to describe many landforms such as the geomorphic evolution of passive margins (Stüwe, 2000).

The diffusion model (Eq. 2.5) assumes proportionality between temporal change and spatial curvature. Despite its simple form, it summarises a range of physical processes such as fluvial incision, hillslope creep and even bedrock landslides. The diffusion model has been very successfully applied in a variety of numerical simulations concerned with the interaction of deformation and erosion (Koons, 1995; Tucker and Slingerland, 1996; Densmore et al., 1998; Willett, 1999; Simpson and Schlunegger, 2003; Simpson, 2004). Persson et al. (2004) used a combination of numerical and sandbox simulations to investigate the topographic evolution of bivergent sand-wedges.

From the above erosion models the elevation dependent erosion law was chosen and implemented to simulate erosion during the sandbox experiments presented in this study. As a second order approach (Stüwe, 2000) it allows to account for results from Willett et al. (1993), who suggested that the location of erosion with respect to the convergence geometry has a significant influence on the distribution and propagation of deformation as well as on the outcrop pattern of metamorphic facies belts. Also, it is emphasised that it was not intended to model the process of erosion itself. Instead, this study is aimed at simulating the effect of erosion on orogenic belts, i. e., unloading with a certain distribution perpendicular to orogenic strike.

Furthermore, an elevation dependent erosion scheme provides a minimum estimate of erosion rates, since Montgomery and Brandon (2002) pointed out that the relation between relief and erosion rate might be better described by a power law. A higher than a minimum estimate of the erosion rates might have exaggerated the effect of erosion on deformation, which was not intended. In addition, an elevation dependent erosion model

has also been successfully applied to (i) numerically simulate the kinematic evolution of bivergent orogens (Pfiffner et al., 2000); (ii) to investigate the effect of erosion on forebulge unconformities (Crampton and Allen, 1995) and (iii) to calculate particle paths trajectories in either bivergent orogens or accretionary wedges (Dahlen and Suppe, 1988; Dahlen and Barr, 1989; Dahlen, 1990; Whipple and Meade, 2004).

The constant erosion model would have been simpler to simulate and considerable experience within sandbox simulations exists. However, this model does not account for the gradient dependence inherent in erosion which should find an expression in the model. Both the slope and the surface curvature dependent erosion models are at present beyond the resolution of this work. At this stage sandbox simulations might be limited by human determined accuracy. We speculate that it would be a key challenge to find a compromise between erosion model (Eq. 2.3) and (Eq. 2.5) to incorporate it in sandbox simulations.